Solvent Effect in the Determination of Brønsted-Evans-Polanyi Relationships for Heterogeneously Catalyzed Reactions

José R. B. Gomes[§,*], Francesc Viñes,[‡] Francesc Illas,[‡] and José L. C. Fajín[≠]

[§]*CICECO – Aveiro Institute of Materials, Departamento de Química, Universidade de Aveiro, Campus Universitário de Santiago, 3810-193 Aveiro, Portugal.*

[‡]*Departament de Química Física & Institut de Química Teòrica i Computacional (IQTCUB), Universitat de Barcelona, c/Martí i Franquès 1, 08028 Barcelona, Spain.*

[≠]*LAQV@REQUIMTE, Faculdade de Ciências, Universidade do Porto, P-4169-007 Porto, Portugal.*

Abstract

Heterogeneous catalyzed reactions take place at the catalyst surface where, depending on the conditions and process, the reacting molecules are either in gas or liquid phase. In the latter case, computational heterogeneous catalysis studies usually neglect solvent effects. In this work, we systematically analyze how the electrostatic contribution to solvent effects influence the atomic structure of reactants and products as well as adsorption, activation and reaction energy for the dissociation of water on several planar and stepped transition metal surfaces. The solvent effects were accounted for through an implicit model that describes the effect of electrostatics, cavitation, and dispersion on the interaction between solute and solvent. The present study shows that activation energy barriers are only slightly influenced by the inclusion of the electrostatic solvent effects accounted for in a continuum solvent approach whereas the adsorption energies of reactants or products are significantly affected. Encouragingly, the linear equations corresponding to the Brønsted-Evans-Polanyi relationships (*BEPs*) relating the activation energies for the dissociation reaction with a suitable descriptor, *e.g.* the adsorption energies of the products of reaction on the difference surfaces, are similar in the presence or in the absence of the solvent. This suggests that BEP relationships derived without the implicit consideration of the solvent are still valid for predicting activation energy barriers of catalytic reactions from a reaction descriptor.

Keywords: Heterogeneous Catalysis; Density Functional Theory; Adsorption; Reaction Descriptors; BEP Relationships; Solvation.

*Corresponding author, e-mail: jrgomes@ua.pt ; Fax: +351 234401470

1. Introduction

Brønsted-Evans-Polanyi relationships (*BEPs*) have long been known as a powerful tool to rationalize chemical reactivity in molecular systems[1,2]. Their use in computational heterogeneous catalysis was introduced nearly 20 years ago by Pallasana and Neurock[3] and since then have been extensively employed[4]. *BEPs* relate the rather difficult to obtain activation energy barrier of an elementary chemical reaction to less computationally demanding descriptors such as reaction or adsorption energy. In the last decades, a significant number of these *BEPs* have been derived for several heterogeneous catalyzed reactions. For example, *BEPs* have been reported for reactions involving metal surfaces where O_2 or N_2 dissociation, ethylene hydrogenation and dehydrogenation on different supported Pd monolayers, acrolein hydrogenation on Pt(111), among others, provide paradigmatic examples[4–8]. Generalization to oxide and carbide surfaces have also been described[9,10].

To obtain *BEPs* requires computational methods able to explore the potential energy surface of interest leading to predictions of adsorption, reaction and activation energy barriers for the network of elementary reactions involved in the process of interest. The workhorse of these studies is Density Functional Theory (*DFT*) and the various available practical implementations. These methods, usually within the generalized gradient approximation (GGA) for the exchange-correlation potential, are broadly used in computational heterogeneous catalysis because of the good compromise between accuracy and computational cost[4,11,12]. *BEPs* are particularly useful to screen catalyst candidates for a target reaction since they allow to predict the activation energy barrier for the reaction of interest on a potential new catalyst model from a given reaction descriptor. Thus, *BEPs* are useful for high-throughput screening of catalysts for a given heterogeneous catalytic reaction.

A particular reaction for which *BEPs* have been derived is water dissociation on metallic[13,14], bimetallic[15], multimetallic surfaces[16] and on platinum nanoparticles[17]. This involved the use of different descriptors and also investigating surfaces with the exposed metal atoms having different Coordination Numbers (*CNs*). The interest in water dissociation comes from its role on the industrially relevant Water Gas Shift (*WGS*) reaction ($CO + H_2O \rightarrow CO_2 + H_2$; ΔH^o = -41 kJ·mol^{-1}), and is also of interest in the liquid phase processing of chemicals. In the WGS reaction, the dissociation of the water molecule is usually regarded normally as the rate limiting

step on flat Cu surfaces[18,19], although detailed kinetic Monte Carlo simulations show that the rate limiting step may change when going to higher temperatures[20] or when the reaction takes place at step sites[21]. For a broad number of surfaces, it was concluded that the adsorption energy of an O adatom or of the products of the water dissociation reaction, OH and H surface species, on the surface model candidate were suitable descriptors[13–17]. These are quantities that can be easily calculated be means of DFT based calculations. Besides, because of the similar linear equations of these *BEPs*, the information gathered in these studies was combined to develop a more general relationship for surface reactions involving breaking the O—H bond in organic molecules on transition metal based catalysts[22]. The *BEP* relationship (*BEPr*) was successfully validated upon comparison of the energy barriers explicitly calculated for the dissociation of formic acid, methanol and ethanol on some of the metal surfaces scrutinized with predictions arising from the use of the *BEPr* and the adsorption energy of the corresponding reaction products (*e.g.* RO and H surface species, with RO=HCOO, CH_3O, CH_3CH_2O, respectively for HCOOH, CH_3OH and CH_3CH_2OH).

One major issue regarding the accuracy of these *BEPs* is the effect of the computational method used. In the recent literature, it is possible to find *BEPs* that were developed from activation energies calculated with different exchange-correlation (*xc*) functionals. In our previous studies, the DFT calculations considered the Perdew-Wang (*PW91*)[23] xc potential within the Generalized Gradient Approximation (*GGA*) but other authors used other *GGA* xc functionals such as the Perdew-Burke-Ernzerhof (*PBE*)[24]. Some recent works even employed functionals from other Jacob's ladder rungs to study heterogeneous reactions on metal surfaces. In a previous study we found that the *PW91* and the *PBE* approaches yielded similar structural and energetic results for the dissociation of the water molecule on the Cu (111) surface[25]. These two functionals also describe the bulk properties of transition metals in a similar way[26]. To investigate the possible transferability of *BEPs* for heterogeneous catalysis, the *BEPs* for the RO—H bond breakage derived from calculations with the *PW91* functional[22] were further recalculated with a more complex, in principle more accurate, xc potential such as the meta-GGA Tao−Perdew−Staroverov−Scuseria (*TPSS*)[27]. In fact *TPSS* was proposed as a good choice for the study of reactions on surfaces due to the simultaneous good description of molecules and bulk properties[28]. Despite the noticeable differences in the energies and geometric parameters obtained with the PW91 and TPSS functionals[29], it was found that the linear equations relating

the activation energies for the breakage of the O—H bonds and the adsorption energies of the products of reaction (RO and H) on several different metal surfaces were very similar, thus concluding that the *BEPs* determined for the RO—H bond breakage[22] is (almost) independent of the density functional used in the calculations[29]. Therefore, that computational study validated the quality and applicability of the previously published *BEPs* and indicated that the activation energy barriers could be determined with less computational expensive density functionals.

In the present study, the electrostatic effects arising from the presence of water as solvent (or other polar molecules) in the energetics of heterogeneously catalyzed reactions are analyzed taking the water dissociation on metal surfaces elementary reaction as a prototype system. This understanding is important because in realistic heterogeneous catalytic scenarios the reactants are often surrounded by other molecules, which may affect the catalytic reactivity through polarization. With this goal in mind, we considered the same surface models previously used to derive the *BEPs* for the reaction of water dissociation on several transition metal surfaces, and calculated new geometries and energies in the presence of an implicit solvent formalism. These data are then compared with the results obtained without the consideration of solvent effects, keeping the remaining computational parameters unchanged. The use of an implicit solvent model may be seen as too crude approximation but it also constitutes the first systematic attempt to investigate the main effects on *BEPs* derived from gas-surface models. Recently, implicit solvent models were employed to analyze the effects of the solvent on several different bond scissions (*e.g.* C–H, O–H, C–C and C–O) that in alcohols on the Pt(111) [30], or the dehydrogenation mechanism of methanol (*e.g.* C–H *vs.* O–H bond cleavage) on solvated Pd, Pt, and Ru surfaces [31]. In the latter work, C-H bond scission was favored and O-H bond scission was disfavored upon consideration of the implicit solvent because, in solution, the CH_3 group of methanol is more exposed to the metal surface atoms than the OH group which is more affected by the solvent electrostatics [31]. In these works it was also found that the combination of implicit and explicit solvation (microsolvation involving just a few solvent molecules) can lead to a solvent description similar to that obtained by inclusion of a rather large number of solvent molecules in the calculations. While the latter is certainly the desirable approach, one must advert that without taking into account the dynamics of the solvent molecules, the description will also be incomplete. The number of degrees of freedom will rapidly increase with the addition of explicit solvent molecules to the molecular models and the establishment of the global minimum would require the consideration of more sophisticated (and computationally more expensive) molecular dynamics or global optimization approaches. To account for this

phenomena or to analyze different implementations of implicit solvent approaches is, however, out of the scope of the present work, which aims at *i)* investigating the purely electrostatic contribution to solvent effect on a rather large number of cases for H_2O dissociation on metal surfaces and *ii)* analyzing whether these electrostatic effects modify the BEP relationships obtained from calculations without solvent effects. Therefore, we will account for an estimate of the mainly electrostatic effects in the catalysis of a simple reaction that are introduced by a continuum solvent model. This arises as a necessary step to forthcoming studies aiming at evaluating the precise role of explicit water in the reaction mechanism.

2. Catalyst surface models and computational details

The *BEPr* for H_2O dissociation, with the implicit inclusion of the solvent effects in the calculations, was obtained through the study of the water dissociation on thirteen planar or stepped Transition Metal (*TM*) surfaces, namely, on the Au(111), Au(321), Ni(111), Cu(111), Pt(111), Pd(111), Ag(110), Cu(110), Cu(321), Ni(110), Ni(211), Pd(110), and Rh(211) surfaces. These surfaces were modelled with slabs of adequate symmetry whose periodic repetition generate the infinite surfaces. The slabs used for the TM(111) and TM(110) surfaces correspond to (2×2) supercells (with respect to the minimal unit cell for these Miller indices) with four atomic layers thickness. The slabs used to generate the TM(211) surfaces correspond to (2×1) supercells while the slabs for the TM(321) surfaces correspond to (1×1) unit cells, also with four atomic layers thickness. The lateral interaction between the adsorbed species and their periodic images in neighboring replicas were found to be lower than 10 meV.

As a common practice, a vacuum region (~10 Å thickness) is introduced in the supercell in the direction perpendicular to the surface to minimize the effect of the surfaces of neighboring periodic replicas; this region has been found to be large enough to avoid any interaction between atoms in consecutive surface slabs[32]. The positions of the metallic atoms in the slabs were obtained through DFT energy minimizations with respect to the geometry. The adsorption sites and their notation in the different surfaces are as shown in Figure 1.

The above described slab models were used in the search of the most stable adsorption configurations for either the reactants (adsorbed water molecule) or the products (co-adsorbed OH and H species) of the water dissociation reaction. This search was done through energy

minimizations with respect to the geometry using the conjugate-gradient algorithm to relax all the atomic coordinates of the adsorbates and the two topmost atomic metallic layers. The atomic coordinates of the metal atoms in the two bottom layers of the slabs were kept frozen to simulate the effect of the bulk crystal on the surface region. Several starting geometries were explored in a systematic way to locate the most stable adsorption configurations. The Dimer approach[33] was used to locate the transition state structures between the most stable configurations of the reactants and of the products. To avoid the algorithm to stop at local minima, especially probable in the case of calculations involving stepped surfaces, very strict convergence criteria (10^{-6} eV for the total energy change and 10^{-3} eV/Å for the forces acting on the ions) were used. The transition states were corroborated by the computation of the vibrational frequencies ensuring the appearance of a single imaginary frequency corresponding to a vibrational mode with associated movement driving from reactants toward products.

All the DFT calculations were carried out with using the VASP code[34–36], and considering the PW91 GGA xc potential[23] to describe the electron density. The use of this density functional allows a direct comparison with the results obtained in previous works[13–17,22].The valence electronic states were described with a plane wave basis set with cutoff of 415 eV for the kinetic energy of the plane waves while the effect of the core electrons in the valence electron density was taken into account using the Projected Augmented-Wave (*PAW*) method as implemented in VASP[37,38]. The numerical integration in the reciprocal space was done using a 7×7×1 Monkhorst-Pack grid of special **k**-points[39]. The convergence of the results with respect to these parameters was already confirmed in a previous work[22]. The effect of the solvent was taken into account through an implicit solvation model as developed by Mathew *et al.*[40,41] describing the effect of electrostatics, cavitation, and dispersion on the interaction between a solute (adsorbates, slab, or adsorbates@slab) and the solvent. The default parameters with a relative permittivity of 80 were employed. Thus, with the exception of the parameters accounting for the implicit solvent approach, the parameters used in the calculations with the implicit solvent were exactly the same as those used in the calculations without considering the solvent effects.

The activation energy barrier (E_{act}) for the water dissociation on each surface was calculated by the difference between the energy of the transition state and that of the initial state (IS, most stable configuration of the reactants on each surface). The reaction energy (E_{react}) was

calculated as the difference between the energy of the final state (FS, most stable geometry for the products on each surface) and that of the IS. The adsorption energies (E_{ads}) for water and OH+H were calculated as $E_{ads} = E_{slab\text{-}adsorbate(s)} - E_{slab} - E_{water}$, where E_{slab} refers to the energy of the metallic surface slab, E_{water} to the energy of H_2O in the gaseous phase, and $E_{slab\text{-}adsorbate(s)}$ refers to the energy of the system where the adsorbate(s) is(are) interacting with the slab. Therefore, in the case of the OH+H co-adsorption, the adsorption energy is given with respect to the energy of the water molecule in the gas phase. The Zero Point Vibrational Energy (*ZPVE*) in the harmonic oscillator approach and considering the vibrational frequencies of the adsorbates in the IS, TS, and FS configurations were added to the energetic quantities above to yield ZPVE-corrected activation energy barriers (E°_{act}), reaction energies (E°_{react}), and adsorption energies (E°_{ads}).

The kinetic constants (k) for the water dissociation reaction were estimated according to the transition state theory[42] through:

$$k = \left(\frac{k_B T}{h}\right)\left(\frac{q^{\neq}}{q}\right) e^{\frac{-E^{o}_{act}}{k_B T}} \qquad (1)$$

where k_B is the Boltzmann constant, T is the absolute temperature for the low temperature WGS reaction (T = 463 K [43]), h the Planck constant, and E°_{act} the activation energy barrier including ZPVE. The $q^{\neq}$ and q are the vibrational partition functions for the TS and IS, respectively, which have been approximated from harmonic vibrational frequencies, obtained via Hessian matrix construction by finite displacements to determine the second derivatives.

3. Results

3.1. Water and OH+H adsorption

Calculated adsorption energies and adsorbate to surface distances for adsorbed water and co-adsorbed OH and H species on the different surfaces considered in this work are reported in Tables 1 and 2, respectively. These values compare the results calculated with the

consideration of an implicit water model, obtained in the present work, with those calculated without the inclusion of the solvent effects, taken from Ref. [22].

On all the considered surface models, the water molecule is found to preferably adsorb on top positions, with its molecular plane parallel to the surface and with the O-H bond lengths at their gas-phase values, *i.e.*, 0.98 Å. This orientation is the preferred one either in the presence or in the absence of the solvent effects. The inclusion of solvent effects in the DFT calculations leads to adsorption energies for the water molecule that are systematically lower (in absolute values) than those calculated without implicit water solvation (Figure 2, compare blue and red triangles). Upon the inclusion of solvent effects, the adsorption of water on the different metallic surfaces becomes slightly less favorable, with adsorption energy differences from calculations with and without solvation effects comprehended in the interval between 0.05 eV, for water adsorption on the Rh(211) surface, and 0.16 eV, for the water adsorption on Cu(111) or Cu(321) surfaces. In the case of TM(111) surfaces, all the top positions are equivalent, while on TM(110) surfaces, because of steric impediments, only a kind of top position is accessible for water adsorption. The stepped TM(211) and TM(321) surfaces present several different top positions, namely, positions at the steps, close to the step edges, and in the middle of the terraces. It is found that on the stepped models, water is preferentially adsorbed at the top positions in the steps where surface atoms present lower coordination numbers. In spite of general decrease of the adsorption energy of the water molecule cause by the presence of the solvent, the distances between the O atom of the water molecule and the nearest surface metal atom (Table 1) become shorter. This rather counterintuitive effect is clearly visible in the radar chart shown in Figure 3 (compare blue and red triangles). The smallest variation in O—surf distance between calculations with and without implicit water effects is found for the Cu(321) surface (0.06 Å), whereas the largest variation is found for the Cu(111) surface (0.22 Å). The water O—H bond lengths are not affected by the inclusion of the solvent effects in the calculations. The reason behind the observed decrease of the distance to the surface is attributed to the repulsion with the solvent reaction field that pushes the adsorbates towards to the surface with a concomitant increase of the Pauli repulsion and a decrease of the adsorption energy.

The most stable positions for the co-adsorption of the OH and H species on each metal surface considered in the present study are not altered upon the inclusion of the solvent effects in the calculations (Table 2). It is seen that OH and H prefer to adsorb at bridge or hollow sites,

being the preference for one or another position dependent not only on the Miller index of the surface but also on the nature of the metallic element. As found for the adsorption of the water molecule, the consideration of solvent effects induces a consistent decrease (0.1 to 0.3 eV) in the strengths of the interactions between the co-adsorbed OH and H species (Table 2 and Figure 2). In what concerns to the nearest-neighbor distances between the OH and H co-adsorbates and metal atoms on the surface, in general, tiny differences are found in between data from the calculations with and without solvent effects (Figure 3). Similarly, the O—H bond length in the OH species is also negligibly affected by the inclusion of the solvent effects.

In summary, the inclusion of the solvent effects in the calculations leads to less favorable interactions with the catalyst surface models as a consequence of the electrostatic screening effect of the solvent.

3.2. O—H bond breakage

The geometrical and energetical results concerning the first O—H bond breakage in the water molecule at the different catalysts surface models considered in the present study are given in Table 3. The transition state structures are only slightly affected by taking solvent effects into account. For instance, in the transition state structures and with the exception of the Au(321) surface model, the O—H length of the cleaved bond is barely affected by inclusion of the solvent effects. The activation energy barriers (E°_{act}) calculated with and without solvent effects differ by less than 0.1 eV, with the exception of the water dissociation on the stepped Cu(321) and Au(321) surfaces, where energy differences of 0.14 eV and 0.25 eV, respectively, are found. With the exception of the Au(111), Pd(111), Pd(110) and Ni(211) surface models, the inclusion of the solvent effects leads to higher activation energies. However, because of the similar activation energies obtained with and without the consideration of solvent effects, these exceptions are barely noticed in Figure 2 (compare green and purple spheres). Nevertheless, despite the slight variation of the calculated activation energy barriers, the inclusion of the solvent effects in the calculations leads to significant changes in the kinetic constant values. In fact, as it can be seen for entries Ag(110) and Cu(321) in Table 3, kinetic constants may change up to two orders of magnitude. As it can be seen in Table 3, the calculated reaction energies (E_{react}) change noticeably upon the inclusion of the solvent effects. These energies become more positive with variations ranging from 0.03 eV, in the case of the Ag(110) surface, to 0.26 eV, in

the case of the Rh(211) surface. Therefore, the inclusion of the solvent effects leads to more endothermic dissociation reaction profiles.

3.3. BEP relationships

In previous studies, the activation energy barriers for the first O—H bond breakage in the water molecule on several metallic surfaces were found to correlate quite well with the adsorption energies of the co-adsorbed OH and H species on the corresponding surfaces [13–17]. However, these results correspond to gas-surface chemistry and, hence, ignores solvent effects. In Figure 4, the *BEPs* obtained from calculated activation energy barriers and co- adsorption energies with and without the consideration of the implicit solvent are compared. Interestingly, the linear correlation obtained from data without consideration of solvent effects, $E^{\circ}_{act} = 0.43 * E^{\circ}_{ads\,(OH+H)} + 0.93$ (values in eV), is almost coincidental to that obtained with data incorporating the implicit solvent effects, $E^{\circ}_{act} = 0.46 * E^{\circ}_{ads\,(OH+H)} + 0.88$. This is because the relationships between the calculated co-adsorption energies of the OH and H species (Figure 5a) and also between the calculated activation energies for the breakage of the O-H bond in the water molecule (Figure 5b) are only marginally affected by the presence of the solvent. Note also that the slopes of the two plots in Figure 5 are close to 1 implying that the overall picture is consistent with the analysis in preceding sections, *i.e.*, the presence of the solvent leads to a decrease in the adsorption energies while the activation energies show a miscellaneous behavior, with the solvent stabilizing more the transition states than the initial structures in some cases, *e.g.* Au(111), Pd(111), and Pd(110), and with the solvent having a distinct behavior in other cases, e.g. in the remaining situations with the exception of Ni(211) for which the activation barrier is the same from calculations with or without the inclusion of the solvent effects. Note that with the exceptions of the Cu(321) and Au(321) surface models, the differences between the activation energy barriers in the presence or in the absence of the implicit solvent are smaller than 0.1 eV, which suggests that, as far as electrostatic contribution is concerned, the solvent effects in the adsorption of the reactants are similar to those in the transition state structures. This had to be expected since the structures of the reactants and of the transition states differ slightly.

4. Conclusions

The effects introduced by the consideration of an implicit solvent in the calculated energetic and geometric data for the species involved in the reaction of water dissociation on several metallic surfaces have been obtained and analyzed. In general, it is found that including solvent effects leads to less favorable adsorbate-surface interactions as a consequence of the electrostatic screening effect introduced by the solvent which pushes the adsorbate to the surface resulting in an increase of the Pauli repulsion between the adsorbate and the metal surface. The activation energy barriers are slightly increased and the dissociation of the O—H bond in the water molecule becomes thermodynamically less favorable (*i.e.*, more endothermic). The differences between these energetic quantities calculated with and without implicit solvents may reach up to 0.3 eV in some cases. Interestingly, the *BEPr* derived from the results calculated with the inclusion of the solvent presents a slope and an intercept that are similar to those of the corresponding relationship obtained from data calculated without solvent effects. This finding clearly evidences the rather local character of the interactions between adsorbates and metallic substrates, and the catalytic substrate effect, thus validating the previous studies evaluating reaction paths and barriers without solvation effects for catalyzed reactions under water environments.

Acknowledgments

This work was developed within the scope of the projects CICECO-Aveiro Institute of Materials, Refs. UID/CTM/50011/2019 and POCI/01/0145/FEDER/007679, and LAQV@REQUIMTE, Refs. UID/QUI/50006/2019 and POCI/01/0145/FEDER/007265 financed by national funds through the Fundação para a Ciência e a Tecnologia (FCT/MCTES) and co-financed by FEDER under the PT2020 Partnership Agreement. The research carried out at the *Universitat de Barcelona* was supported by the Spanish MINECO/FEDER CTQ2015-64618-R and, in part, by *Generalitat de Catalunya* (grants 2017SGR13 and XRQTC). F.V. thanks the MINECO for a postdoctoral *Ramón y Cajal* (RyC) research contract (RYC-2012-10129), and F.I. acknowledges additional support from the 2015 ICREA Academia Award for Excellence in University Research. Additional financial support from Spanish Ministerio de Ciencia, Investigación y Universidades (MICIUN) through the Excellence *María de Maeztu* program (grant MDM-2017-0767) is also fully acknowledged.

Table 1. ZPVE corrected DFT adsorption energies, E^{o}_{ads}, in eV, and distances in between O and the nearest metal surface atom, *d*(O-Surf), in Å, for the H_2O adsorption on metallic surfaces. Second row corresponds to the data determined taken into account the effect of the solvent. Site notation as in Figure 1. ΔE^{o}_{ads} and Δ_d quantify the extent of solvent effects.

Surface	Site	E^{o}_{ads}	ΔE^{o}_{ads}	*d*(O-Surf)	Δ_d
Au(111)	top "t"	-0.18	0.12	2.90	-0.11
	top "t"	-0.06		2.79	
Ni(111)	top "t"	-0.31	0.12	2.23	-0.14
	top "t"	-0.19		2.09	
Cu(111)	top "t"	-0.22	0.16	2.50	-0.22
	top "t"	-0.06		2.28	
Pt(111)	top "t"	-0.27	0.09	2.51	-0.20
	top "t"	-0.18		2.31	
Pd(111)	top "t"	-0.30	0.10	2.45	-0.12
	top "t"	-0.20		2.33	
Cu(110)	top "t"	-0.42	0.11	2.19	-0.07
	top "t"	-0.31		2.12	
Ni(110)	top "t"	-0.53	0.12	2.11	-0.09
	top "t"	-0.41		2.02	
Pd(110)	top "t"	-0.48	0.13	2.31	-0.10
	top "t"	-0.35		2.21	
Ag(110)	top "t"	-0.32	0.13	2.53	-0.08
	top "t"	-0.19		2.45	
Ni(211)	top "1"	-0.61	0.13	2.09	-0.10
	top "1"	-0.48		1.99	
Rh(211)	top "1"	-0.55	0.05	2.29	-0.08
	top "1"	-0.50		2.21	
Cu(321)	top "1"	-0.58	0.16	2.14	-0.06
	top "1"	-0.42		2.08	
Au(321)	top "1"	-0.34	0.07	2.57	-0.16
	top "1"	-0.27		2.41	

Table 2. ZPVE corrected DFT adsorption energies, E^{o}_{ads}, in eV, and distances in between OH and H to nearest metal surface, *d*(OH/H-Surf) and in between O and H atoms in OH species, *d*(O-H), in Å, for the OH + H co-adsorbed situations on metallic surfaces. Second row corresponds to the data determined taken into account the effect of the solvent. Site notation as in Figure 1. ΔE^{o}_{ads} and Δ_d quantify the extent of solvent effects.

	OH/H Sites	E^{o}_{ads}	ΔE^{o}_{ads}	*d*(OH/H-Surf)	*d*(O-H)
Au(111)	bridge "b" / hollow	1.59	0.13	2.27; 2.37 / 1.89; 1.91; 1.83	0.98
	bridge "b" / hollow	1.72		2.26; 2.39 / 1.89; 1.92; 1.82	0.98
Ni(111)	hollow "f" / hollow	-0.68	0.21	1.97; 1.97; 1.97 / 1.68; 1.68; 1.68	0.97
	hollow "f" / hollow	-0.47		1.92; 1.92; 1.92 / 1.67; 1.67; 1.67	0.98
Cu(111)	hollow "h" / hollow	-0.07	0.27	2.02; 2.06; 2.06 / 1.69; 1.70; 1.69	0.97
	hollow "h" / hollow	0.20		2.00; 2.04; 2.04 / 1.69; 1.70; 1.69	0.98
Pt(111)	bridge "b" / hollow	0.39	0.23	2.18; 2.18 / 1.89; 1.79; 1.89	0.98
	bridge "b" / hollow	0.62		2.16; 2.16 / 1.89; 1.80; 1.89	0.98
Pd(111)	hollow "f" / hollow	0.11	0.23	2.17; 2.17; 2.17 / 1.80; 1.80; 1.80	0.97
	hollow "f" / hollow	0.34		2.14; 2.14; 2.14 / 1.80; 1.80; 1.80	0.98
Cu(110)	bridge "b" / hollow	-0.38	0.20	1.97; 1.97 / 1.71; 1.70; 1.75	0.97
	bridge "b" / hollow	-0.18		1.98; 1.98 / 1.71; 1.71; 1.75	0.97
Ni(110)	bridge "b" / hollow	-1.05	0.24	1.92; 1.92 / 1.69; 1.70; 1.70	0.98
	bridge "b" / hollow	-0.81		1.90; 1.90 / 1.69; 1.69; 1.68	0.98
Pd(110)	bridge "b" / hollow	-0.31	0.23	2.11; 2.11 / 1.82; 1.82; 1.80	0.98
	bridge "b" / hollow	-0.08		2.11; 2.11 / 1.81; 1.82; 1.80	0.98
Ag(110)	bridge "b" / hollow	0.50	0.18	2.23; 2.23 / 1.97; 1.87; 1.87	0.98
	bridge "b" / hollow	0.68		2.27; 2.27 / 1.97; 1.87; 1.87	0.97
Ni(211)	bridge "b" / hollow	-1.31	0.25	1.91; 1.91 / 1.69; 1.70; 1.71	0.98
	bridge "b" / hollow	-1.06		1.89; 1.89 / 1.69; 1.69; 1.69	0.98
Rh(211)	bridge "b" / bridge	-0.96	0.31	2.10; 2.10 / 1.75; 1.75	0.98
	bridge "b" / bridge	-0.65		2.10; 2.10 / 1.75; 1.75	0.98
Cu(321)	bridge "$b_{4\text{-}1}$" / hollow	-0.36	0.32	1.95; 1.95 / 1.63; 1.76; 1.78	0.97
	bridge "$b_{4\text{-}1}$" / hollow	-0.04		2.07; 1.89 / 1.63; 1.76; 1.78	0.98
Au(321)	bridge "$b_{1\text{-}2}$" / bridge	0.84	0.25	2.25; 2.12 / 1.65; 1.86	0.98
	bridge "$b_{1\text{-}2}$" / bridge	1.09		2.24; 2.12 / 1.66; 1.85	0.98

Table 3. Activation energy barrier, E^{o}_{act}, in eV, and imaginary frequencies, **ν,** in cm^{-1}, for the transition state, and distance, *d*(O-H), in Å, for the O-H bond breaking, reaction rate constants, *k*, obtained at 463 K, in s^{-1}, and reaction energies, E_{react}, in eV, for the H_2O dissociation reaction on several metallic surfaces. Second row corresponds to the data determined taken into account the effect of the solvent. ΔE^{o}_{act} and ΔE^{o}_{react} quantify the extent of solvent effects.

Surface [a]	**ν**	*d*(O-H)	Δ_d	E^{o}_{act}	ΔE^{o}_{act}	*k*	E^{o}_{react}	ΔE^{o}_{react}
Au(111)	347i	2.01	0.00	1.88	-0.03	1.5×10^{-9}	1.64	0.13
	325i	2.01		1.85		3.9×10^{-8}	1.77	
Ni(111)	747i	1.55	0.01	0.71	0.03	7.4×10^{4}	-0.37	0.09
	863i	1.54		0.74		2.5×10^{4}	-0.28	
Cu(111)	1234i	1.47	0.00	0.91	0.10	1.6×10^{2}	0.15	0.11
	1276i	1.47		1.01		3.3×10^{1}	0.26	
Pt(111)	244i	1.78	0.02	0.78	0.02	5.1×10^{3}	0.66	0.14
	251i	1.80		0.80		3.2×10^{3}	0.80	
Pd(111)	532i	1.70	-0.02	0.96	-0.06	5.1×10^{1}	0.41	0.13
	560i	1.68		0.90		1.2×10^{2}	0.54	
Cu(110)	1262i	1.43	0.02	0.61	0.08	4.0×10^{5}	0.03	0.10
	1306i	1.45		0.69		5.0×10^{4}	0.13	
Pd(110)	882i	1.50	0.01	0.73	-0.04	6.9×10^{3}	0.17	0.11
	944i	1.51		0.69		3.1×10^{4}	0.28	
Ni(110)	1273i	1.34	0.02	0.39	0.04	1.8×10^{8}	-0.52	0.12
	1333i	1.36		0.43		3.8×10^{7}	-0.40	
Ag(110)	901i	1.64	0.00	1.12	0.07	2.2×10^{1}	0.85	0.03
	968i	1.64		1.19		1.2×10^{-1}	0.87	
Ni(211)	946i	1.32	0.00	0.61	0.00	1.1×10^{6}	-0.70	0.14
	1047i	1.32		0.61		7.9×10^{5}	-0.56	
Rh(211)	1086i	1.47	-0.02	0.67	0.06	1.2×10^{5}	-0.41	0.26
	1105i	1.45		0.73		4.6×10^{4}	-0.15	
Cu(321)	820i	1.63	-0.03	0.71	0.14	3.6×10^{4}	0.22	0.16
	956i	1.60		0.85		2.8×10^{2}	0.38	
Au(321)	392i	1.86	0.29	1.33	0.25	3.5×10^{-3}	1.19	0.18
	168i	2.15		1.58		5.5×10^{-4}	1.37	

Figure 1. Possible adsorption sites at the TM(111); TM(110); TM(211), and TM(321) surfaces. Labels are t: top; b: bridge; h: hcp hollow; f: fcc hollow; c3: three-fold site at steps, c4: four-atoms hollow site at steps. Numbers are used to distinguish different top and bridge sites on the same model surface.

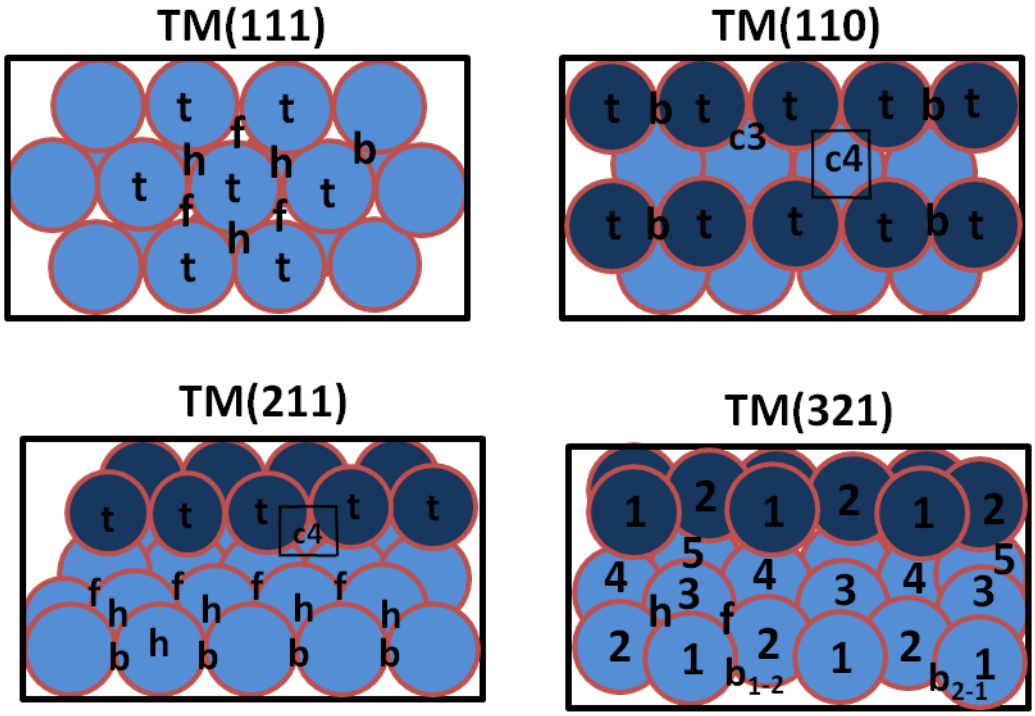

Figure 2. Comparison of the calculated activation energies for first O-H bond breakage in the water molecule, E^{o}_{act} (HO---H), and of the adsorption energies for the water molecule, E^{o}_{ads} (H_2O), and for the co-adsorbed OH and H species, E^{o}_{ads} (OH+H), with and without the consideration of the solvent. The numbers in red correspond to energies in eV.

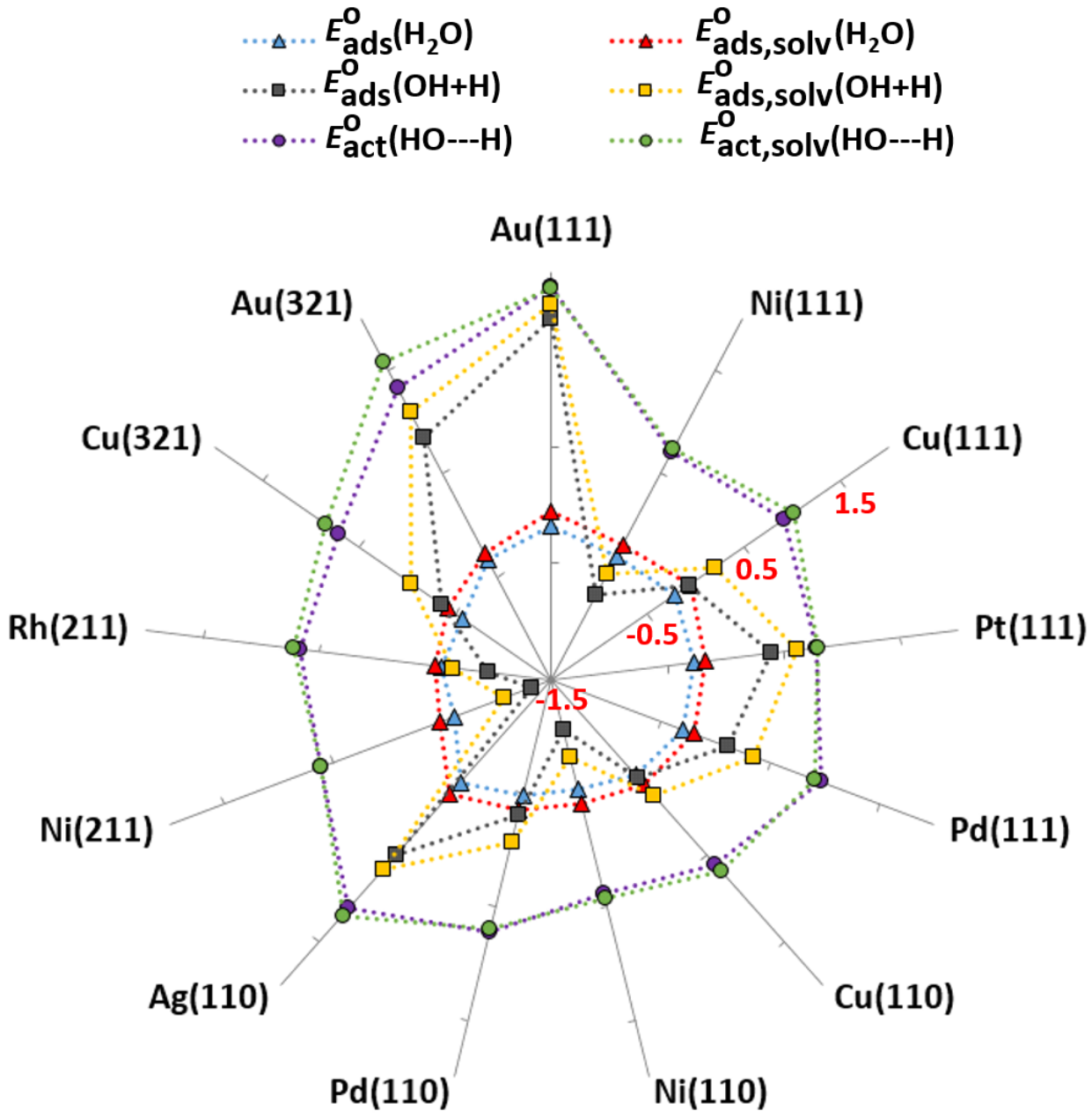

Figure 3. Comparison of the optimized adsorbate (water and co-adsorbed OH and H species) to surface nearest-neighbor distances with and without the consideration of the solvent. The numbers in red correspond to interatomic distances in Å.

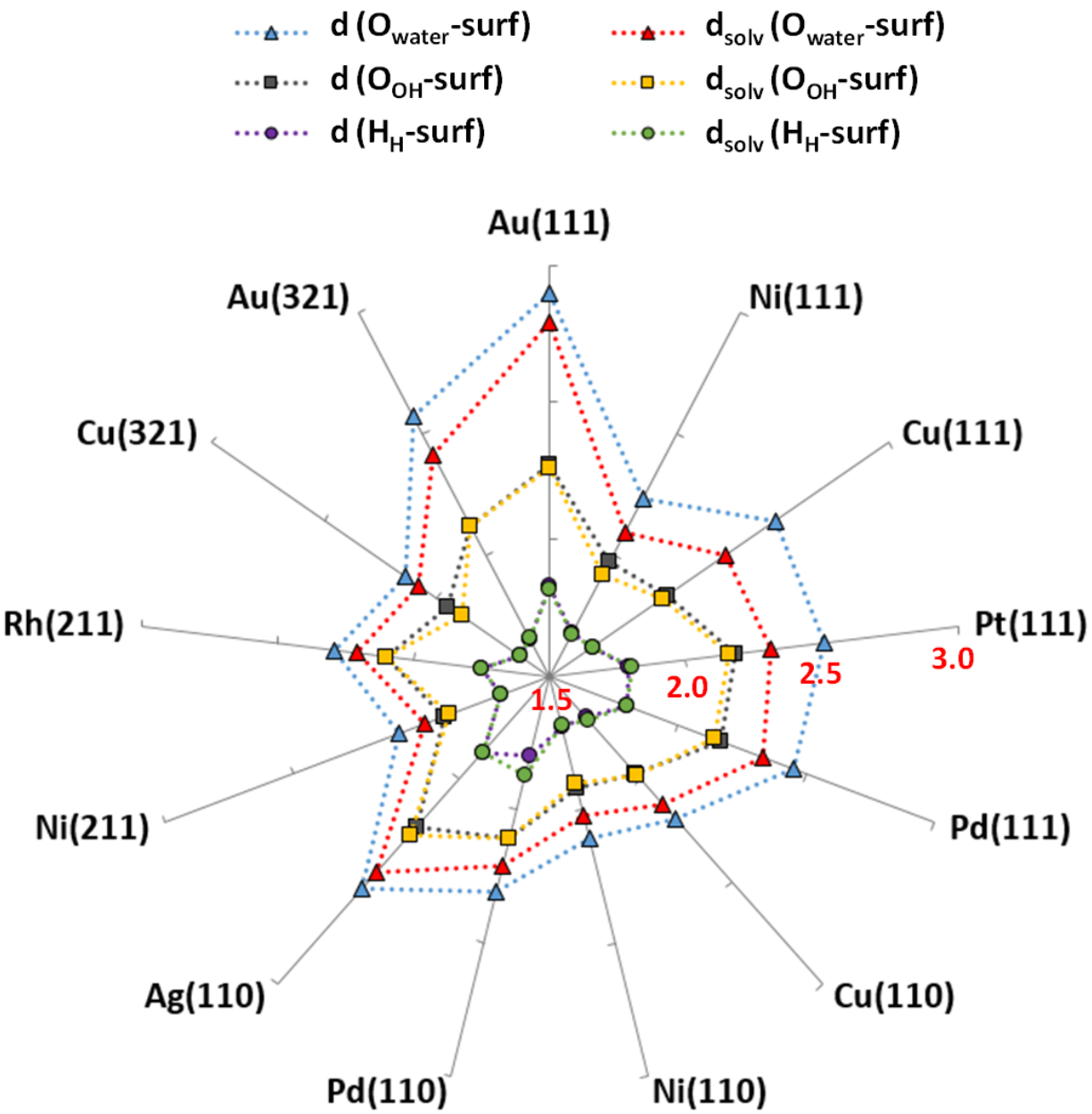

Figure 4. Activation energy barriers, E^{o}_{act}(HO---H), versus co-adsorption energies E^{o}_{ads}(OH+H), of the products of the reaction $H_2O^* + * \rightarrow HO^* + H^*$ on several metallic surfaces calculated with (red) or without (blue) including implicit solvent effects.

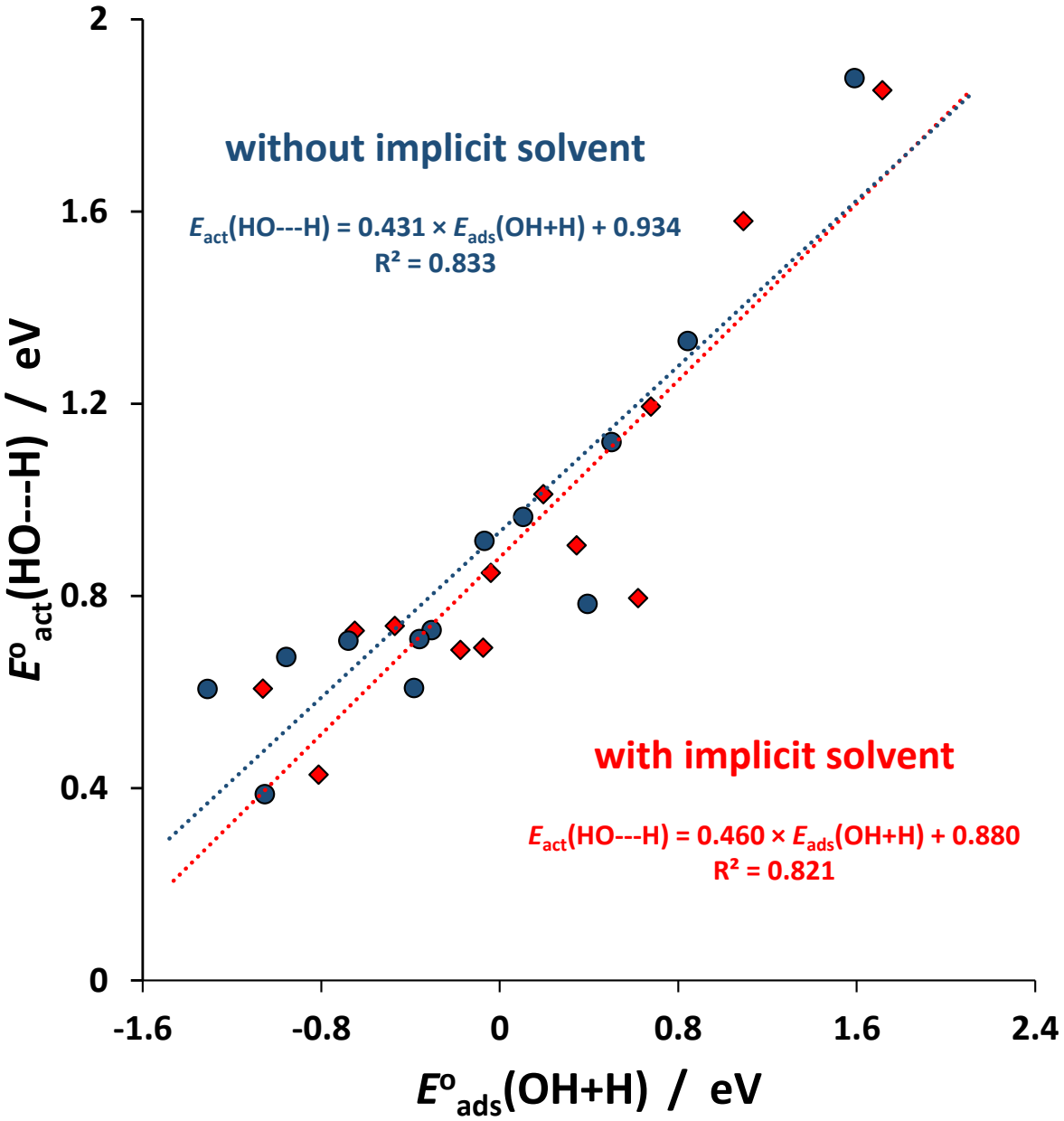

Figure 5. Comparison of the calculated co-adsorption energies of OH and H species (a) and of the activation energy barriers for the dissociation of the O-H bond in the water molecule (b) with (horizontal axis) and without (vertical axis) the implicit solvent formalism.

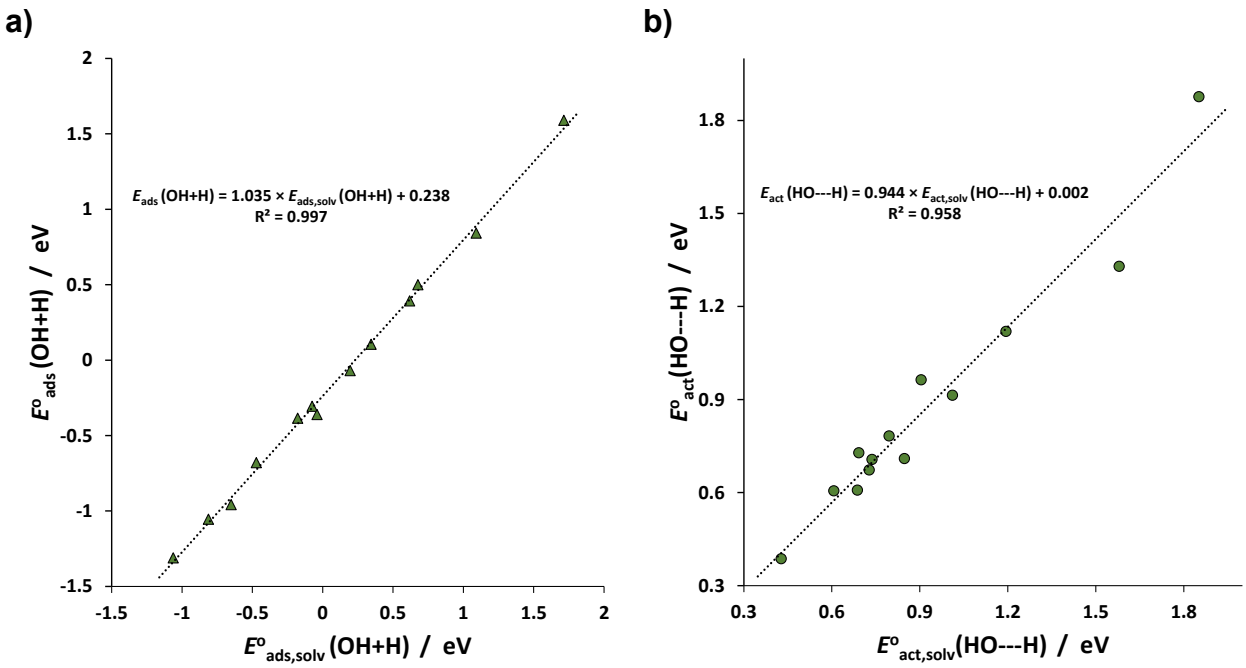

References

1 J. N. Bronsted, Acid and Basic Catalysis., *Chem. Rev.*, 1928, **5**, 231–338.

2 M. G. Evans and M. Polanyi, Inertia and driving force of chemical reactions, *Trans. Faraday Soc.*, 1938, **34**, 11.

3 V. Pallassana and M. Neurock, Electronic Factors Governing Ethylene Hydrogenation and Dehydrogenation Activity of Pseudomorphic PdML/Re(0001), PdML/Ru(0001), Pd(111), and PdML/Au(111) Surfaces, *J. Catal.*, 2000, **191**, 301–317.

4 J. K. Nørskov, F. Studt, F. Abild-Pedersen and T. Bligaard, *Fundamental Concepts in Heterogeneous Catalysis*, 2014.

5 J. K. Nørskov, T. Bligaard, A. Logadottir, S. Bahn, L. B. Hansen, M. Bollinger, H. Bengaard, B. Hammer, Z. Sljivancanin, M. Mavrikakis, Y. Xu, S. Dahl and C. J. H. Jacobsen, Universality in Heterogeneous Catalysis, *J. Catal.*, 2002, **209**, 275–278.

6 D. Loffreda, F. Delbecq, F. Vigné and P. Sautet, Fast Prediction of Selectivity in Heterogeneous Catalysis from Extended Brønsted-Evans-Polanyi Relations: A Theoretical Insight, *Angew. Chemie Int. Ed.*, 2009, **48**, 8978–8980.

7 R. A. van Santen, M. Neurock and S. G. Shetty, Reactivity Theory of Transition-Metal Surfaces: A Brønsted–Evans–Polanyi Linear Activation Energy–Free-Energy Analysis, *Chem. Rev.*, 2010, **110**, 2005–2048.

8 R. A. Van Santen, Complementary Structure Sensitive and Insensitive Catalytic Relationships, *Acc. Chem. Res.*, 2009, **42**, 57–66.

9 F. Viñes, A. Vojvodic, F. Abild-Pedersen and F. Illas, Brønsted–Evans–Polanyi Relationship for Transition Metal Carbide and Transition Metal Oxide Surfaces, *J. Phys. Chem. C*, 2013, **117**, 4168–4171.

10 A. Vojvodic, F. Calle-Vallejo, W. Guo, S. Wang, A. Toftelund, F. Studt, J. I. Martínez, J. Shen, I. C. Man, J. Rossmeisl, T. Bligaard, J. K. Nørskov and F. Abild-Pedersen, On the behavior of Brønsted-Evans-Polanyi relations for transition metal oxides, *J. Chem. Phys.*, 2011, **134**, 244509.

11 J. R. B. Gomes, J. L. C. Fajín, M. N. D. S. Cordeiro, C. Teixeira, P. Gomes, R. S. Pillai, G. Novell-Leruth, J. Toda and M. Jorge, in *Density Functional Theory: Principles, Applications and Analysis*, eds. J. Maurin and J. M. Pelletier, Nova Science Publishers, Inc., New York, First Edit., 2013, pp. 1–58.

12 K. Duanmu and D. G. Truhlar, Validation of Density Functionals for Adsorption Energies on Transition Metal Surfaces, *J. Chem. Theory Comput.*, 2017, **13**, 835–842.

13 J. L. C. Fajín, M. N. D. S. Cordeiro, F. Illas and J. R. B. Gomes, Descriptors controlling the catalytic activity of metallic surfaces toward water splitting, *J. Catal.*, 2010, **276**, 92–100.

14 J. L. C. Fajín, M. N. D. S. Cordeiro and J. R. B. Gomes, Density Functional Theory Study of the Water Dissociation on Platinum Surfaces: General Trends, *J. Phys. Chem. A*, 2014, **118**, 5832–5840.

15 J. L. C. Fajín, M. N. D. S. Cordeiro and J. R. B. Gomes, Water Dissociation on Bimetallic Surfaces: General Trends, *J. Phys. Chem. C*, 2012, **116**, 10120–10128.

16 J. L. C. Fajín, M. N. D. S. Cordeiro and J. R. B. Gomes, Water dissociation on multimetallic catalysts, *Appl. Catal. B Environ.*, 2017, **218**, 199–207.

17 J. L. C. Fajín, A. Bruix, M. N. D. S. Cordeiro, J. R. B. Gomes and F. Illas, Density functional theory model study of size and structure effects on water dissociation by platinum nanoparticles, *J. Chem. Phys.*, 2012, **137**, 034701.

18 A. A. Gokhale, J. A. Dumesic and M. Mavrikakis, On the Mechanism of Low-Temperature Water Gas Shift Reaction on Copper, *J. Am. Chem. Soc.*, 2008, **130**, 1402–1414.
19 J. L. C. Fajín, M. N. D. S. Cordeiro, F. Illas and J. R. B. Gomes, Influence of step sites in the molecular mechanism of the water gas shift reaction catalyzed by copper, *J. Catal.*, 2009, **268**, 131–141.
20 H. Prats, L. Álvarez, F. Illas and R. Sayós, Kinetic Monte Carlo simulations of the water gas shift reaction on Cu(111) from density functional theory based calculations, *J. Catal.*, 2016, **333**, 217–226.
21 H. Prats, P. Gamallo, F. Illas and R. Sayós, Comparing the catalytic activity of the water gas shift reaction on Cu(321) and Cu(111) surfaces: Step sites do not always enhance the overall reactivity, *J. Catal.*, 2016, **342**, 75–83.
22 J. L. C. Fajín, M. N. D. S. Cordeiro, F. Illas and J. R. B. Gomes, Generalized Brønsted–Evans–Polanyi relationships and descriptors for O–H bond cleavage of organic molecules on transition metal surfaces, *J. Catal.*, 2014, **313**, 24–33.
23 J. P. Perdew, J. A. Chevary, S. H. Vosko, K. A. Jackson, M. R. Pederson, D. J. Singh and C. Fiolhais, Atoms, molecules, solids, and surfaces: Applications of the generalized gradient approximation for exchange and correlation, *Phys. Rev. B*, 1992, **46**, 6671–6687.
24 J. P. Perdew, K. Burke and M. Ernzerhof, Generalized Gradient Approximation Made Simple, *Phys. Rev. Lett.*, 1996, **77**, 3865–3868.
25 J. L. C. Fajín, F. Illas and J. R. B. Gomes, Effect of the exchange-correlation potential and of surface relaxation on the description of the H_2O dissociation on Cu(111), *J. Chem. Phys.*, 2009, **130**, 224702.
26 P. Janthon, S. M. Kozlov, F. Viñes, J. Limtrakul and F. Illas, Establishing the Accuracy of Broadly Used Density Functionals in Describing Bulk Properties of Transition Metals, *J. Chem. Theory Comput.*, 2013, **9**, 1631–1640.
27 J. Tao, J. P. Perdew, V. N. Staroverov and G. E. Scuseria, Climbing the Density Functional Ladder: Nonempirical Meta–Generalized Gradient Approximation Designed for Molecules and Solids, *Phys. Rev. Lett.*, 2003, **91**, 146401.
28 P. Janthon, S. (Andy) Luo, S. M. Kozlov, F. Viñes, J. Limtrakul, D. G. Truhlar and F. Illas, Bulk Properties of Transition Metals: A Challenge for the Design of Universal Density Functionals, *J. Chem. Theory Comput.*, 2014, **10**, 3832–3839.
29 J. L. C. Fajín, F. Viñes, M. N. D. S. Cordeiro, F. Illas and J. R. B. Gomes, Effect of the Exchange-Correlation Potential on the Transferability of Brønsted–Evans–Polanyi Relationships in Heterogeneous Catalysis, *J. Chem. Theory Comput.*, 2016, **12**, 2121–2126.
30 B. Schweitzer, S. N. Steinmann and C. Michel, Can microsolvation effects be estimated from vacuum computations? A case-study of alcohol decomposition at the H 2 O/Pt(111) interface, *Phys. Chem. Chem. Phys.*, 2019, **21**, 5368–5377.
31 M. Garcia-Ratés, R. García-Muelas and N. López, Solvation Effects on Methanol Decomposition on Pd(111), Pt(111), and Ru(0001), *J. Phys. Chem. C*, 2017, **121**, 13803–13809.
32 L. Vega, J. Ruvireta, F. Viñes and F. Illas, Jacob's Ladder as Sketched by Escher: Assessing the Performance of Broadly Used Density Functionals on Transition Metal Surface Properties, *J. Chem. Theory Comput.*, 2018, **14**, 395–403.
33 G. Henkelman and H. Jónsson, A dimer method for finding saddle points on high dimensional potential surfaces using only first derivatives, *J. Chem. Phys.*, 1999, **111**, 7010–7022.

34 G. Kresse and J. Hafner, Ab initio molecular dynamics for liquid metals, *Phys. Rev. B*, 1993, **47**, 558–561.
35 G. Kresse and J. Furthmüller, Efficiency of ab-initio total energy calculations for metals and semiconductors using a plane-wave basis set, *Comput. Mater. Sci.*, 1996, **6**, 15–50.
36 G. Kresse and J. Furthmüller, Efficient iterative schemes for ab initio total-energy calculations using a plane-wave basis set, *Phys. Rev. B*, 1996, **54**, 11169–11186.
37 P. E. Blöchl, Projector augmented-wave method, *Phys. Rev. B*, 1994, **50**, 17953–17979.
38 G. Kresse and D. Joubert, From ultrasoft pseudopotentials to the projector augmented-wave method, *Phys. Rev. B*, 1999, **59**, 1758–1775.
39 H. J. Monkhorst and J. D. Pack, Special points for Brillouin-zone integrations, *Phys. Rev. B*, 1976, **13**, 5188–5192.
40 K. Mathew, R. Sundararaman, K. Letchworth-Weaver, T. A. Arias and R. G. Hennig, Implicit solvation model for density-functional study of nanocrystal surfaces and reaction pathways, *J. Chem. Phys.*, 2014, **140**, 084106.
41 K. Mathew and R. G. Hennig, Implicit self-consistent description of electrolyte in plane-wave density-functional theory.
42 Keith J Laidler, *Chemical Kinetics*, Harper Collins, New York, 3rd edn., 1987.
43 J. L. Ayastuy, M. A. Gutiérrez-Ortiz, J. A. González-Marcos, A. Aranzabal and J. R. González-Velasco, Kinetics of the Low-Temperature WGS Reaction over a $CuO/ZnO/Al_2O_3$ Catalyst, *Ind. Eng. Chem. Res.*, 2005, **44**, 41–50.